Assessing Confidence Level in Synchrophasor-based Fault Location Results Using Goodness of Fit Metrics

Matin Rahmatian[1], Yu Christine Chen[2], William G. Dunford[3], Farnoosh Rahmatian[4]
[1]Specialist Power System Consultants,
[1, 2, 3] University of British Columbia,
[4]NuGrid Power Corp.
Email: [1]matin.rahmatian@pscconsulting.com, [2]chen@ece.ubc.ca, [3]wgd@ece.ubc.ca [4]frahmatian@nugridpower.com
Canada

SUMMARY

Synchrophasors obtained from phasor measurement units (PMUs) feed various real-time and off-line applications through wide-area measurement systems. The accuracy of synchrophasors, especially during transient-state operating conditions, such as during-fault and immediate post-fault periods, may affect the reliability or credibility of the results obtained from the applications. Recently, a goodness of fit (GoF) metric has been introduced that can show a quantitative quality of the fit (or correlation) between the original sampled waveform and the waveform regenerated using the calculated phasor quantities, i.e., amplitude, phase, and frequency [1]. This metric was further extended to be calculated after the removal of the decaying DC component of the signal and was applied to a real-time fault location application [2]. Through various case studies, it is shown that the GoF and its variant form called $\overline{\text{GoF}}$ are correlated with the fault location results' errors. In other words, higher levels of GoF and/or $\overline{\text{GoF}}$ correlate with higher accuracy and higher credibility for fault location results [3].

1. INTRODUCTION

Use of time synchronized voltage and current measurements can serve a number of functions in electric power systems. There is growing interest in using synchrophasor systems, providing voltage and current phasors time-tagged to an absolute (common) time, to enable a plurality of real-time and non-real-time applications. In the recent years, there has been a tremendous amount of research, development, and pilot demonstrations of various applications using synchrophasor data. For production grade applications, however, reliable performance is often very critical. IEEE Std. C37.118-2005 [4] and its later versions (e.g., IEEE Std C37.118.1-2011 [5] and IEEE Std C37.118.1a-2014 [6]) specify certain quality flags and performance requirements for PMUs; however, these performance requirements may not be sufficient for certain applications. For example, the accuracy of a PMU during transient conditions on a faulted line is not well defined. In fact, describing a waveform which is not a simple periodic sinusoidal waveform is not possible using the basic phasor definition. Generally, some of the cases leading to non-sinusoidal waveforms are:

- DC offsets (decaying DC) during the early cycles of faults with long time constants,
- Amplitude jumps in the first cycle of fault,
- Distortions due to current transformer (CT) saturation,

- Distorted waveforms during high-impedance faults,
- Noise in the measured signal, especially at low currents (low signal-to-noise ratio).

Such discrepancies can lead to significant errors in applications that use these measurements. Accordingly, using synchrophasor measurements during a transient condition may lead to unreliable results as the measurements may not be reasonable representations of the voltage and current waveforms on the line.

Recently, a GoF metric has been introduced that can show the fit (or correlation) between the original sampled waveform and the waveform regenerated using the calculated phasor quantities, i.e., amplitude, phase, and frequency [1]. Using the phasor magnitude, frequency, and phase information from a phasor measurement unit (PMU), we can recover a corresponding reconstructed time-domain signal. Suppose PMU phasor measurements are reported at intervals of Δt, i.e., at times $t_k = k\Delta t$, $k = 1, 2, \ldots$ The reconstructed a-phase voltage and current waveforms are expressed as

$$v_m^a(t) = |V_m^a[k]|.\cos\left(\omega_m^a[k]t + \emptyset_m^a[k]\right),$$

$$i_{(m,n)}^a(t) = \left|I_{(m,n)}^a[k]\right|.\cos\left(\omega_m^a[k]t + \theta_m^a[k]\right),$$

where $(k-1)\Delta t < t \leq k\Delta t$. $v_m^a(t)$ is the regenerated (re-constructed) phase voltage waveform at bus *m,* at time *t* and $i_{(m,n)}^a(t)$ is the regenerated current in line *(m,n)* at time *t.* Moreover, $|V_m^a[k]|$ and $\left|I_{(m,n)}^a[k]\right|$ denote measured voltage and current phasors, $\omega_m^a[k]$ shows the measured frequency at $t_k = k\Delta t$. Similarly, $\emptyset_m^a[k]$ and $\theta_{(m,n)}^a[k]$ are the voltage and current phases measured by the PMU.

Next, considering the actual sampled voltage and current waveforms as $\hat{v}_m^a(t)$ and $\hat{\imath}_{(m,n)}^a(t)$, the difference between the regenerated and the actual would be

$$\Delta v_m^a(t) = v_m^a(t) - \hat{v}_m^a(t)$$

$$\Delta i_{(m,n)}^a(t) = i_{(m,n)}^a(t) - \hat{\imath}_{(m,n)}^a(t)$$

Such discrepancies can be represented by the GoF as a single quantity over the measurement window *k*. The GoF metric (in [dB]) for the *a*-phase voltage and current are computed as

$$\varphi_m^a[k] = 20\,log\frac{|V_m^a[k]|}{\sqrt{\frac{1}{N-M}\sum_{j=1}^{N}(\Delta v_m^a(t_{k-1} + j\Delta\tau))^2}}$$

$$\psi_{(m,n)}^a[k] = 20\,log\frac{|I_{(m,n)}^a[k]|}{\sqrt{\frac{1}{N-M}\sum_{j=1}^{N}(\Delta i_{(m,n)}^a(t_{k-1} + j\Delta\tau))^2}}$$

where N represents the number of samples in one measurement window (166 samples here) and M represents the number of estimated parameters used to reconstruct the waveform. In our setting, $M = 3$, where the estimated parameters are amplitude, phase, and frequency.

In the next section, via a numerical example, we illustrate how the GoF metric quantifies the mismatch between the PMU phasor measurement and the corresponding actual time-domain signal and how it can be applied to assess the credibility of the fault location results.

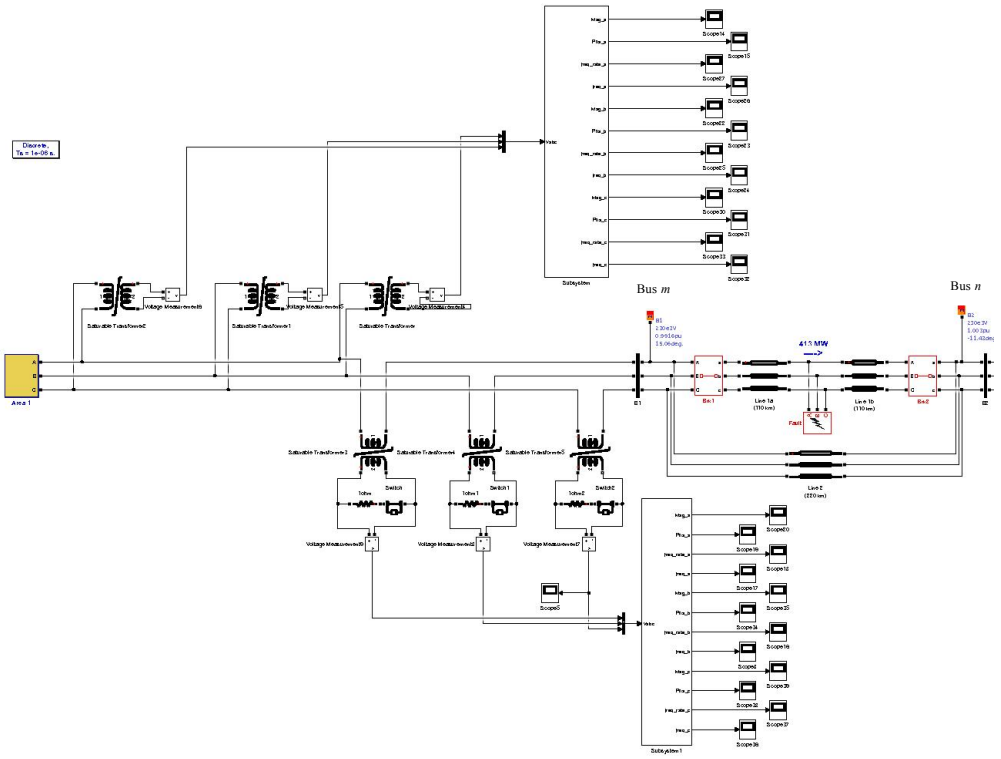

Fig. 1. Part of two-area power system with VT, CT and PMU models simulated in MATLAB Simulink.

2. Application of GoF to the Credibility of Fault Location Results

In this section, we consider the canonical two-area test power system shown in Fig. 1. Particularly, we are interested in one of the two identical 230-kV three-phase balanced transmission lines of length 220km connecting the two areas via buses *m* and *n*. A transposed distributed line model is used to simulate the transmission line. The PMUs are modelled in the MATLAB Simulink environment using the FFT function at the nominal 60-Hz frequency to obtain phasor magnitudes and phase angles. Then, these values are reported once per electrical cycle, i.e., t = 16.667 ms. Four P-class PMU models are connected to both ends of the test transmission line using current and voltage transformer models, part of which is shown in Fig. 1. Then, we use the voltage- and current-phasor measurements obtained at steady state to compute the positive-, negative-, and zero-sequence impedance values as $Z_{s,}$(m,n) = [116.8884∠243°; 116.88∠84.243°; 617.59∠55.004°] .

Next, we try to answer the arisen question on how the fault-location application can assess the credibility of its results. We choose a simulation case of 3-phase to ground fault (*abcg*). Unbeknownst to operators, the fault occurs at 60 km from bus *m* with fault-to-ground resistance 5 Ω at time t = 0 s, and the fault sustains for three cycles before circuit breakers are tripped. Phasor measurements are collected at times $t_k = k\Delta t$, k = 1, 2, 3, i.e., at the end of each electrical cycle during the fault. We also assume that the GoF is calculated by the PMU at each measurement window in pre-, during-, and post-fault periods. The current waveform obtained at terminal 1 is shown in Fig. 2. The current waveform reconstructed from phasor measurements is depicted by the dash-dot trace, while the original current signal is represented by the solid trace. We observe that the current waveform reconstructed from phasor measurements reasonably matches the actual signal in the third cycle during the fault, but not the first. Such discrepancies can lead to significant errors in applications that use these measurements, as we reveal in Example 2 with respect to fault location.

The GoF quantities are evaluated in each measurement window, marked by circles in Fig. 2. Based on a visual examination of Fig. 2, we can say the in the pre-fault period ($k \leq 0$), the waveform reconstructed using PMU measurements matches the actual waveform obtained from simulations. In this period where the mismatch is minimal, evaluated GoFs $\psi^a_{(m,n)}[k] \approx 50$ dB or better, $k \leq 0$. In during-fault period ($1 \leq k \leq 3$), Immediately following the fault initiation time $t = 0$ s, the mismatch between the actual and reconstructed waveforms grows, so that the GoF evaluated in the first during-fault cycle is $\psi^a_{(m,n)}[1] = 7.5$ dB. As the transients settle in measurement windows $k = 2, 3$, the match between the two waveforms improves, and the GoF correspondingly increase to $\psi^a_{(m,n)}[k] = 19$ dB for $k = 2$, and $\psi^a_{(m,n)}[k] = 31$ dB for $k = 3$. Finally, Post-fault period ($k > 3$): After 3 cycles, i.e., at t = 50 ms, the fault is cleared by opening circuit breakers at both ends of the faulted line at near zero current. Following the disconnection of one line, the current through that line decreases sharply. Again, such a sudden change causes the mismatch between the waveforms to increase, and in turn leads to lower GoF in measurement window $k = 4$.

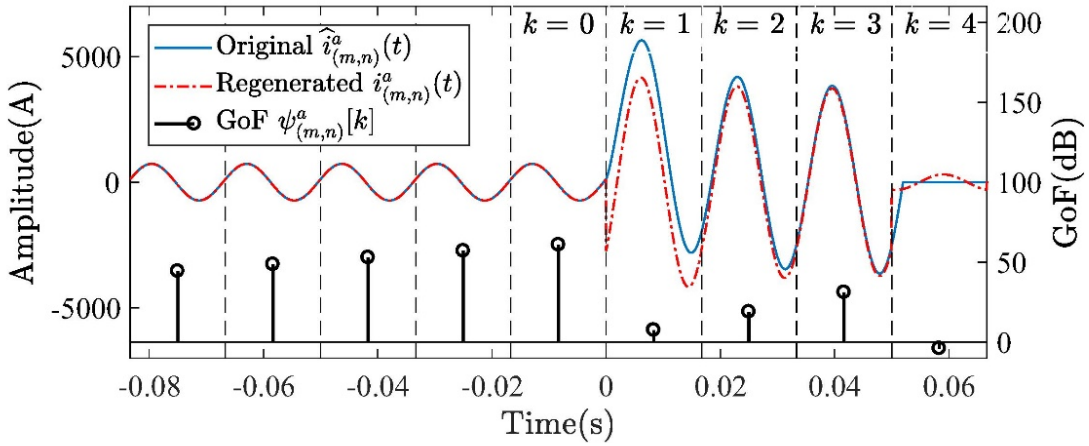

Fig. 2. Phase-a actual current waveform and that reconstructed from PMU phasor measurements

The obtained results are summarized in Table 1. Considering the third cycle, i.e., in measurement window $2\Delta t < t \leq 3\Delta t$, the estimated distances (locations of fault) are nearly identical to the actual location (60 km) with errors of less than 0.1% normalized to the line length of 220 km. On the other hand, the table reports fault location results obtained using data from the first cycle of the during fault, too. By comparing the results obtained for the third and first cycles of the during-fault period, we find that the results from the former are much more accurate than those in the latter. Of particular concern is that errors in the estimated fault location grows from less than 0.1% to more than 2.0%, a sizeable increase.

Table 1. Fault location estimation using measurements from the first and third cycle of during-fault period for phase *a*, *b* and *c*.

Applied cycle	$d^a[k]$		$d^b[k]$		$d^c[k]$	
	km	%Error	km	%Error	km	%Error
$k = 1$	64.999	2.223	61.023	0.465	57.978	0.919
$k = 3$	60.060	0.027	60.080	0.036	60.007	0.003

2.1. Accounting for DC Offset Effect on GoF Results

As discussed in Introduction section, one reason of the mismatch is DC offsets (decaying DC) during the early cycles of faults with long time constants. We investigate this issue in this subsection more. Assume that in measurement window k, the PMU measuring the current at a-phase in line (m,n) is able to calculate the DC offset for current as

$$\Delta\bar{i}^{a}_{(m,n)}[k] = \frac{1}{N}\sum_{j=1}^{N} \Delta i^{a}_{(m,n)}\,(t_{k-1} + j\Delta\tau)$$

These can be interpreted as the mean value of the difference between the actual and reconstructed signals in measurement window k. Now, using the DC-offset information in conjunction with PMU phasor measurements (i.e., amplitude, phase, and frequency), we hope that the reconstructed waveforms would more closely match the actual ones. Therefore, we can calculate the new form of GoF for current as

$$\bar{\psi}^{a}_{(m,n)}[k] = 20\,log\,\frac{|I^{a}_{(m,n)}[k]|}{\sqrt{\frac{1}{N-M}\sum_{j=1}^{N}((\Delta i^{a}_{(m,n)}(t_{k-1} + j\Delta\tau) - \Delta\bar{i}^{a}_{(m,n)}[k])^2}}$$

Now, we consider the same system and fault scenario as in Section 2.1., but in addition to $|I^{a}_{(m,n)}[k]|$, $\theta^{a}_{(m,n)}[k]$, and $\omega^{a}_{m}[k]$, assume that the DC offset is available. The reconstructed current waveform is superimposed onto the actual one in Fig. 2b. In this case, in contrast to Fig. 2, the reconstructed and actual waveforms match much more closely, with the greatest improvement in the during-fault period, especially in measurement window $k = 1$. Correspondingly, as compared with Example 3, GoF values are greater in the during-fault period, as depicted in Fig. 2b. Specifically, in the problematic measurement window $k = 1$ from Example 3, the GoF increases from 7.5 dB to 20.5 dB.

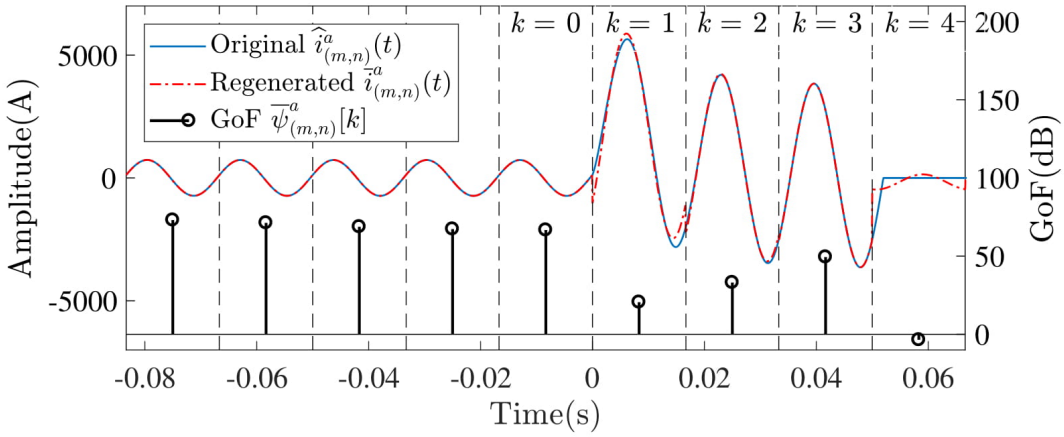

Fig. 2. Phase-a actual current waveform and that reconstructed from PMU phasor measurements after DC-offset compensation

Based on the discussion above, we propose to include the GoF and its DC-offset-modified variant as prescribed quantities for the PMU to transmit to real-time applications. In the proposed structure, in addition to the phasor information (amplitude, phase, and frequency) reported by the standard PMU, the GoF and $\overline{\text{GoF}}$ (which denotes the GoF -variant that quantifies the mismatch between the original signal and the one reconstructed accounting for DC-offset) are also computed and transmitted. It is worth noting that we do not advocate to transmit the DC-offset itself to the application, because our goal is not to reconstruct the actual voltage and current waveforms at the application, but rather to determine whether or not real-time application results using phasors are credible. Next, via numerical case studies, we illustrate how the GoF metrics can help to assess the performance quality of the fault-location application.

3. Case Studies

To assess the confidence level in the obtained results, we have modeled a three-phase transmission line with the length of 220 km and simulated five types of fault, i.e., *abcg*, *abg*, *ag*, *ab*, and *abc* type faults at 10, 60, 110, 160, and 210 km from one end of the line. We have also modelled a typical P-class PMU

capable of measuring current and voltage of each phase at both ends of the line. Through the PMU models, we have access to the measured synchrophasors per electrical cycle during the pre-fault, during-fault (lasting three cycles), and post-fault periods. To have consistent and thorough results, we have simulated all the faults with 11 different initiation times distributed equally in the first cycle of the during-fault period. Calculating the fault locations from synchrophasor data for all three cycles of the during-fault period, we have 2475 results or cases. For each case, we can calculate an absolute fault location error normalized to the length of line while having the GoF values.

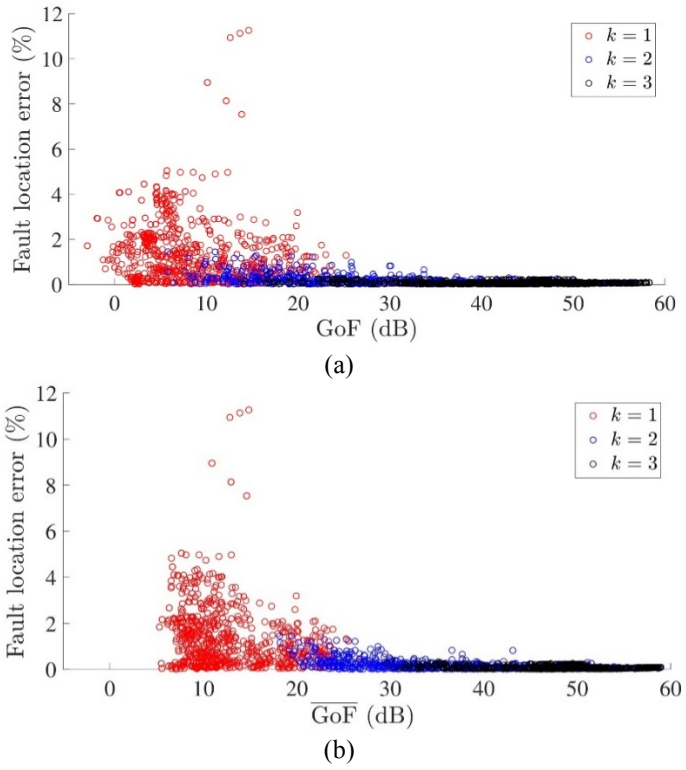

Fig. 3. Fault location error versus GoF values computed for waveforms reconstructed from PMU phasor measurements obtained in the three cycles of during-fault periods (a) in original form and (b) after DC-offset remove for simulated cases.

In this work, we extend our investigation on the synchrophasor-based fault location process and interpret the results more tangibly for field implementation. The plots in Fig. 3 shows the fault location errors versus GoF and $\overline{\text{GoF}}$ to demonstrate the correlation between GoF metrics and the fault location errors. Generally, fault location errors are better when using synchrophasor data with higher GoF and $\overline{\text{GoF}}$ values (preferably over 30 or 35 dB). Fig. 4 shows the distribution of the cases as a function of GoF and $\overline{\text{GoF}}$, showing the number of cases with higher (e.g., >30 dB) goodness of fit are higher when $\overline{\text{GoF}}$ is used (hence $\overline{\text{GoF}}$ is preferred). Fig. 5 shows the distribution of the 95-percentile error levels versus GoF indices (i.e., fault location errors for 95% of the cases in each 2-dB bin is less than the indicated value). It demonstrates how the confidence level in fault location accuracy improves with higher values of GoF indices and how quantitative quality-indicators such as goodness of fit parameters are useful (or perhaps necessary) for building rugged (high confidence level) production-grade applications based on synchrophasor data. Fig. 5, or a fitted curve to the data in Fig. 5, can be used in a practical synchrophasor-based fault location application to provide tolerance (2-sigma uncertainty levels) for the fault location data reported to the operators.

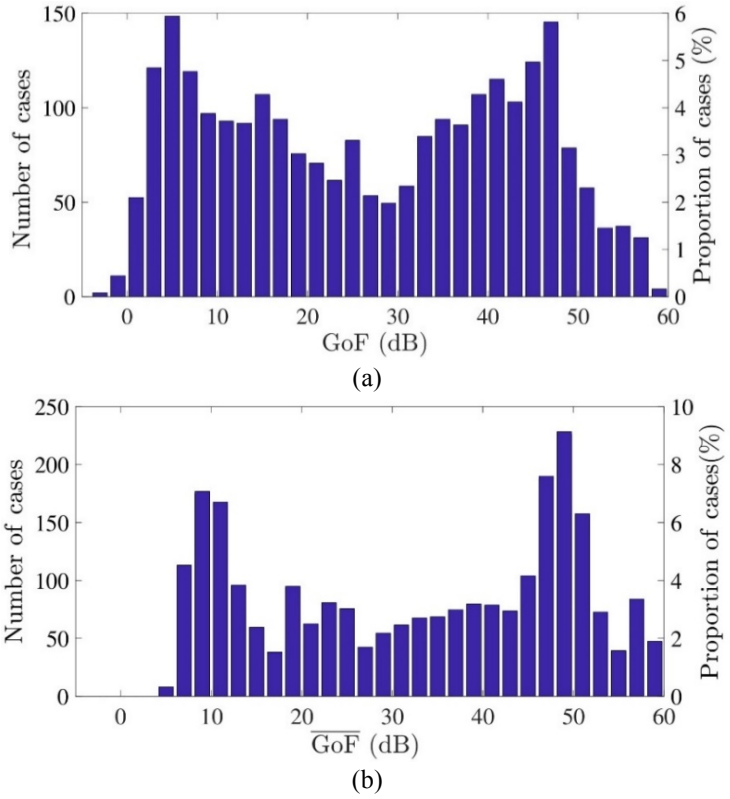

Fig. 4. Distribution of the number or proportion (percent) of cases versus their GoF values in 2-dB steps (bins) (a) in original form and (b) after DC-offset remove for simulated cases.

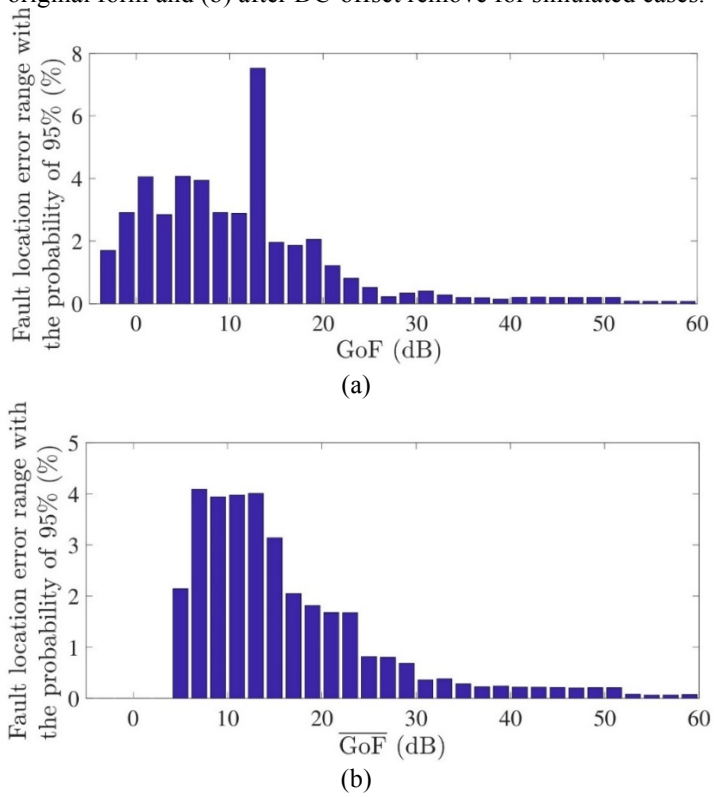

Fig. 5. Distribution of 95-percentile fault location error values versus GoF values (a) in original form and (b) after DC-offset remove for simulated cases.

4. CONCLUSIONS

Quantitative metrics such as Goodness-of-Fit can be very beneficial tools in building reliable power system applications using synchrophasor data. As the industry transitions from research and early application demonstrations to production-grade products using synchrophasor data, it is important to support the evolution of the digital measurement technology with distributed quantitative measures of data quality. The local (distributed) quality metric calculation helps with managing the cost of extra computation power (a benefit of edge computing). The availability of quantitative quality metrics allows a range of applications to use the same synchrophasor data (i.e., reduced data acquisition cost per application) through filtering useful data at/for each specific application based on the thresholds or confidence levels needed for that specific application.

BIBLIOGRAPHY

[1] A. Riepnieks and H. Kirkham, "An introduction to goodness of fit for PMU parameter estimation," *IEEE Transactions on Power Delivery*, vol. 32, no. 5, pp. 2238-2245, Oct. 2017.

[2] M. Rahmatian, Y. C. Chen, W. G. Dunford, and F. Rahmatian, "Incorporating Goodness-of-fit Metrics to Improve Synchrophasor-based Fault Location," *IEEE Transactions on Power Delivery*, Available Online, doi: 10.1109/TPWRD.2018.2790410, 2018.

[3] M. Rahmatian, Y. C. Chen, W. G. Dunford, and F. Rahmatian, "Synchrophasor data qualification measures for reliable fault location," *in Proc. of PAC World North America Conference*, Raleigh, NC, August 2017.

[4] "IEEE standard for synchrophasors for power systems" *IEEE Std C37.118-2005*.

[5] "IEEE standard for synchrophasor measurements for power systems," *IEEE Std C37.118.1-2011 (Revision of IEEE Std C37.118-2005)*.

[6] "IEEE standard for synchrophasor measurements for power systems – amendment 1: Modification of selected performance requirements," *IEEE Std C37.118.1a-2014 (Amendment to IEEE Std C37.118.1-2011)*.